

VI. AnBi. Actinide monobismuthides

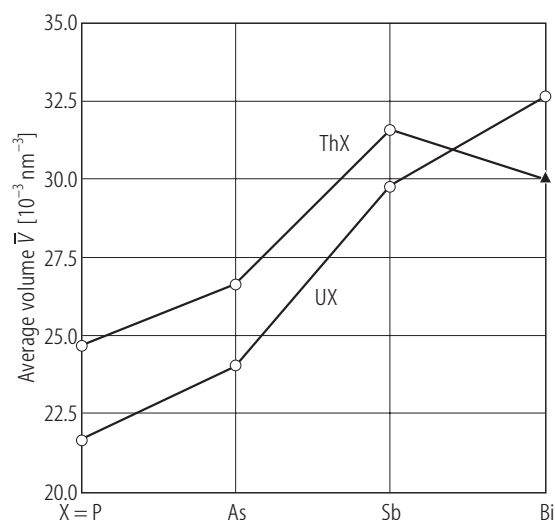


Fig. VI.1. ThBi, UBi. Average atomic volumes of thorium and uranium monobismuthides compared to the remaining mononitrides except for mononitrides [82BBF]. Open circles – NaCl-type, closed triangles – CsCl-type.

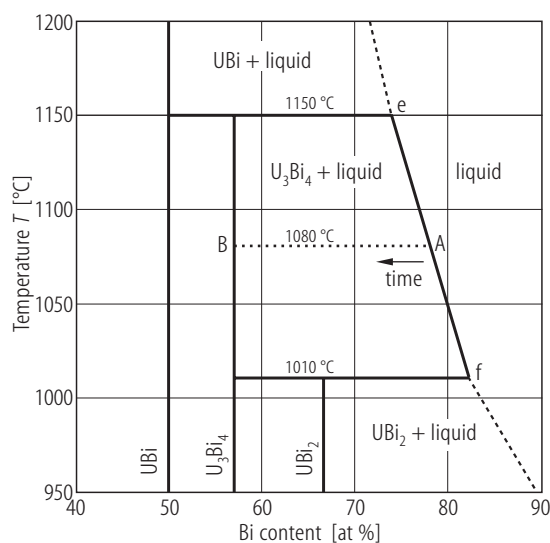


Fig. VI.2. U-Bi. Phase diagram [81CAA]. UBi is formed in peritectic reaction at about 1150 $^{\circ}\text{C}$. Due to its enormous piroforic tendency and problems to get actinide monobismuthides in a single crystalline form only little information is available in the literature.

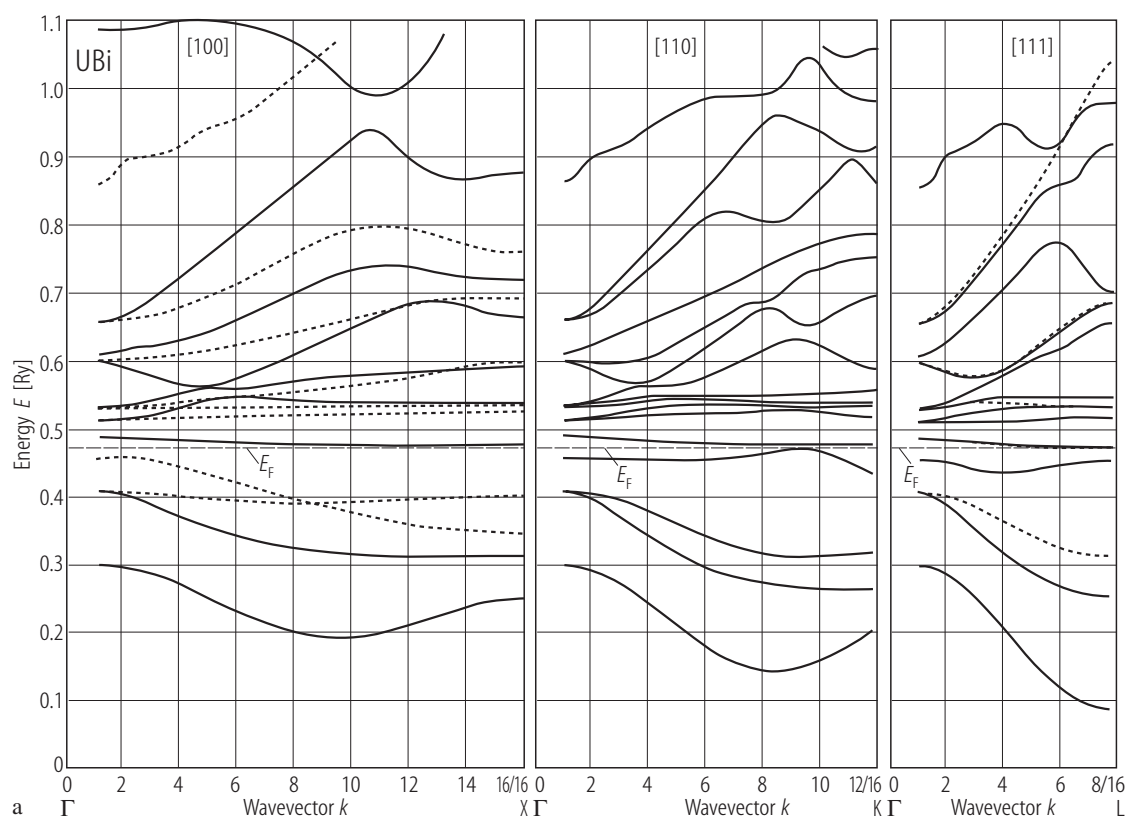


Fig. VI.3a. For caption see p. 408

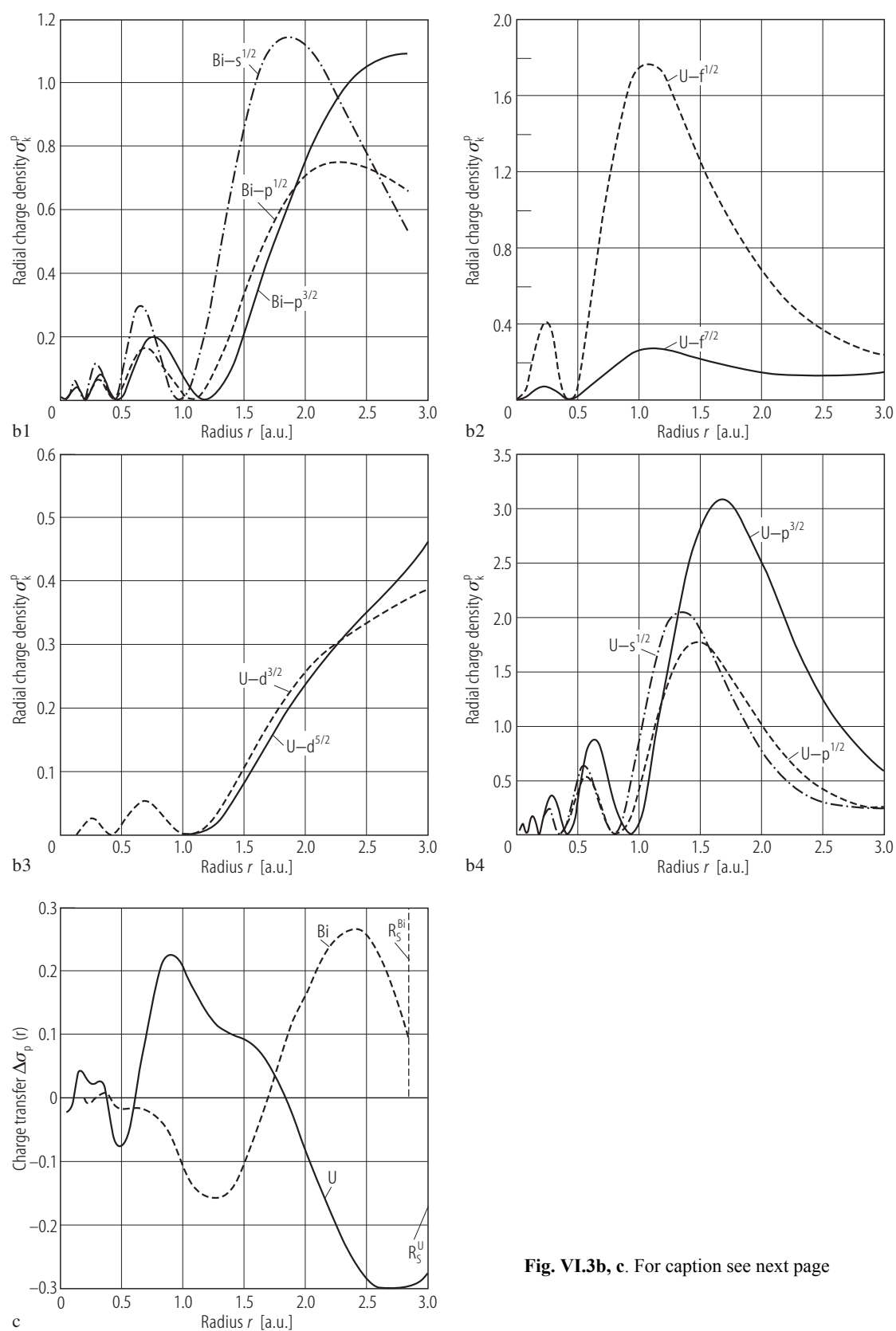


Fig. VI.3b, c. For caption see next page

Fig. VI.3. UBi. **(a)** Self-consistent, RKKR-type energy bands using the X_α -exchange potential [82WPN]. Left hand panel: along the k-ray [100], Γ - Δ -X (the point Γ is denoted by 0, the point X by 16/16). Middle panel: along the k-ray [110], Γ - Σ -K, K is 12/16. Right hand panel: along the k-ray [111], Γ - Δ -L, L is 8/16. All principal reciprocal space directions are in units $\pi/8a$. One can see between 1.13 eV and 5.45 eV below the Fermi level three overlapping energy bands which are mainly the 6p states but have also d and f symmetry in the U-sphere. This emphasizes the existence of the exceptionally large anisotropy, which is attributed to bonding between the pnictogen p-electrons and U 5f electrons. **(b)** The radial charge densities $\sigma_k^p(r)$ of the U f(7/2, 5/2), U d(5/2, 3/2), U p(3/2, 1/2) and U s(1/2) states as well as of the Bi p(3/2, 1/2) and Bi-s(1/2) states [82WPN]. **(c)** The charge transfer occurring on compound formation. Radial charge density difference $\Delta\sigma_p(r) = \sigma_p(r) - \sigma_p^{\text{at. S}}(r)$ within muffin tin spheres vs. the distance r from the origin of the respective sphere [82WPN]. $\sigma_p(r)$ is the total charge density and $\sigma_p^{\text{at. S}}(r)$ is the radial charge density obtained by superposing the relativistic atomic charge densities of the neutral neighbouring atoms. Note for the U-sphere a maximum at 0.9 a.u. and minimum at about 2.7 a.u. The maximum coincides with the peaks in the $f^{5/2}$ - $f^{7/2}$ -like radial charge density (see figure (b)). This indicates an increase in f-like charge density in the U-sphere, being about half an electron larger than in the case of UN. The minimum in $\Delta\sigma_U(r)$ is related to the $d^{5/2}$ - and $d^{3/2}$ -like radial charge densities, while the peak in the $\Delta\sigma_{\text{Bi}}(r)$ curve at about 2.4 a.u. corresponds to the maximum of the $p^{3/2}$ - and $p^{1/2}$ -like radial charge density in the Bi-sphere. R_s^p denotes the muffin tin sphere radius.

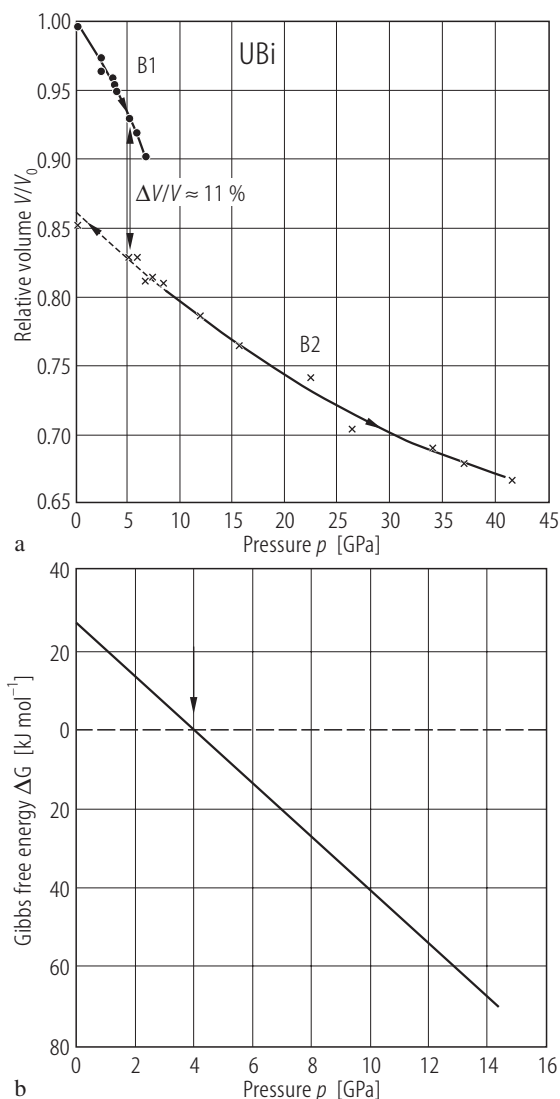


Fig. VI.4. UBi. **(a)** Relative volume, V/V_0 , vs. pressure, p , up to 42 GPa [92BDDG], [93GHBH]. $a_0 = 0.63627$ nm. The onset of the B1→B2 transition occurs at 5 GPa. $B_0 = 91(4)$ GPa, $B'_0 = -5(3)$. The latter negative value points to some electronic interaction changing continuously with pressure like for the samarium monochalcogenides. Note that the formed CsCl-type structure (B2) is retained to the maximum pressure studied, while the B2 phase is retained down to normal pressure after the release. This retention of the high-pressure phase is related to that in USb [89GSBD]. **(b)** Gibbs free energy (ΔG) against pressure, p , the high-pressure behaviour in UBi is studied by a theoretical model based on an interatomic potential approach under the framework of charge transfer effects arising from three-body interaction [03JS]. The calculated compression curves and the values of the transitions reproduce well the experimental results [93GHBH].

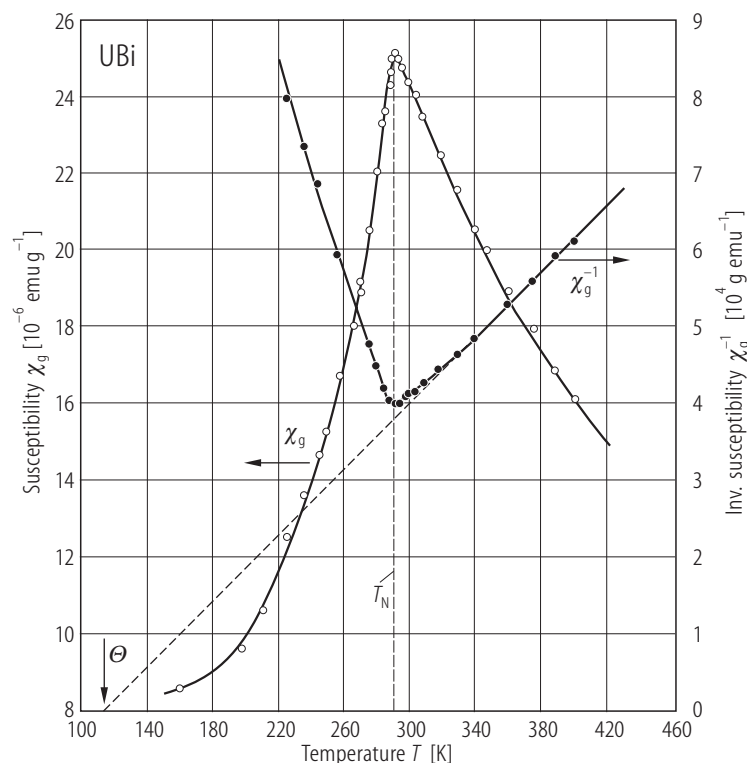


Fig. VI.5. UBi. Specific magnetic susceptibility, χ_g , and inverse magnetic susceptibility, χ_g^{-1} , both as a function of temperature [66TZ]. $a_0 = 0.6397 \text{ nm}$. The magnetic behaviour of UBi is dependent on the cooling rate: 1) by rapid quenching from 800°C the specimen is antiferromagnetic below $T_N = 290 \text{ K}$, the highest one among actinide compounds (see Fig. R.11). $\Theta = 115 \text{ K}$, $p_{\text{eff}} = 4.06 \mu_B$; 2) by cooling slowly from 800°C the specimen shows up ferromagnetic properties with $T_C = 156 \text{ K}$ (the ferromagnetic phase U_3Bi_4 has $T_C = 108 \text{ K}$). Simultaneously new diffraction lines occur indicating a formation of different crystal structure.

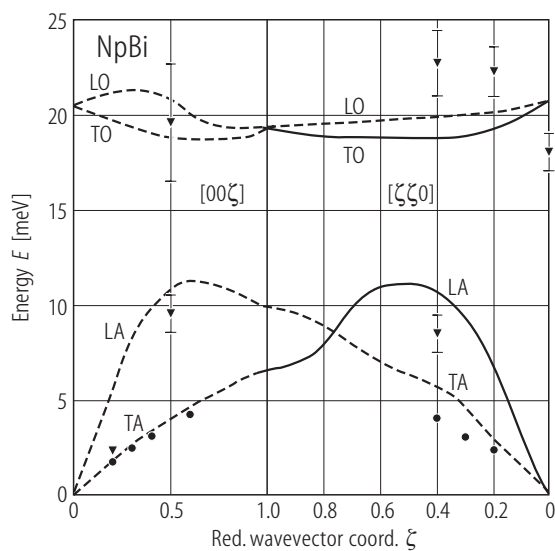


Fig. VI.6. NpBi s.c. Phonon dispersion diagram [97BBBF]. The dashed lines are the USb phonon dispersion curves taken from [79LSV2], while the filled triangle and circle symbols correspond to longitudinal (L) and transverse (T) phonons of NpBi, respectively. LA and TA as well as LO and TO denote the corresponding acoustic and optic modes, respectively.

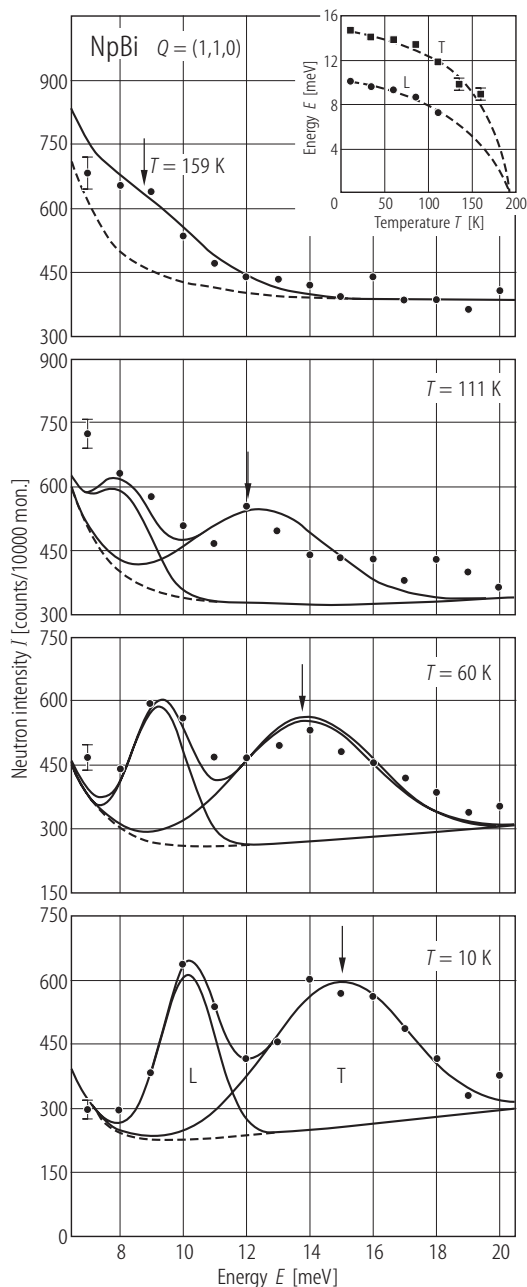


Fig. VI.7. NpBi s.c. Energy scans at constant $Q=(1,1,0)$ measured at temperatures between 10 and 159 K, far below T_N ($= 192.5$ K) [97BBBF]. A constant function is used to fit the excitation (solid lines). The dashed lines show the background contribution. Note that for this Q -value both longitudinal (L) and transverse (T) modes are observed. The absence of the low-energy excitation at $Q=(0,0,1)$ (not shown), for which only transverse excitations contribute, proves its longitudinal character. As shown by [81JB], the presence of a low-energy branch with a longitudinal polarization (being a component of transverse mode) is a signature of triple- \mathbf{k} ordering (see Fig. R.16). The inset gives the temperature dependences of the longitudinal L and transverse T modes.

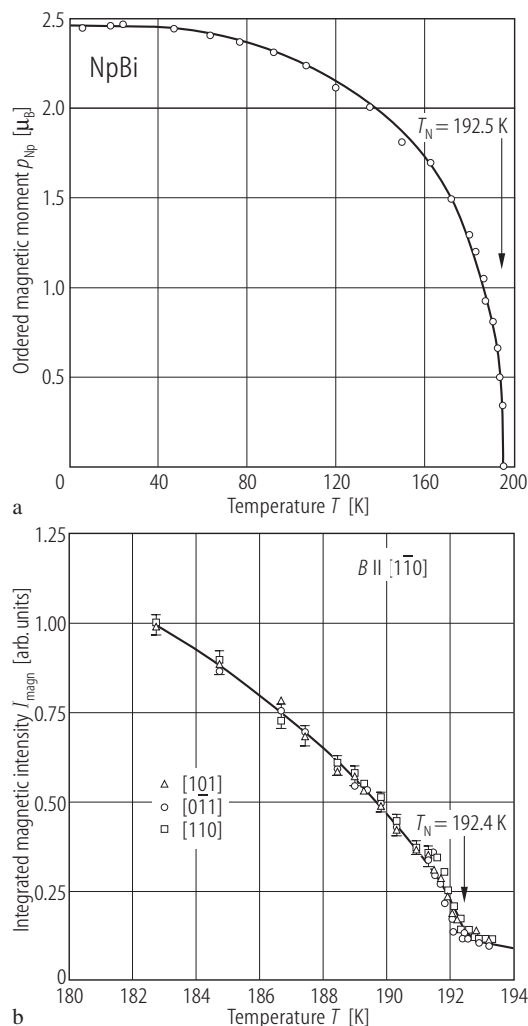


Fig. VI.9. NpBi s.c. (a) Ordered magnetic moment, p_{Np} , vs. temperature, T , in zero applied magnetic field determined by neutron scattering [92BBRS]. All three equivalent \mathbf{k} -vectors $[001]$, $[010]$ and $[100]$ have the same intensity and hence the same values of Fourier components $m_{\mathbf{k}i} = 1.40(7) \mu_B$. This in any case gives the Np ordered moment $p_{\text{Np}} = \sqrt{3} m_{\mathbf{k}i} = 2.48(1) \mu_B$. $T_N = 192.5$ K. (b) Neutron magnetic intensities I_{magn} measured along the $[1\bar{1}0]$ axis in a magnetic field of 4.6 T [92BBRS]. Note that the magnetic intensities arising from three equivalent \mathbf{k} -vectors measured by cooling below T_N , have the same values and the same temperature dependence. This proves the triple- \mathbf{k} type ordering in NpBi.

For Fig. VI.8 see next page

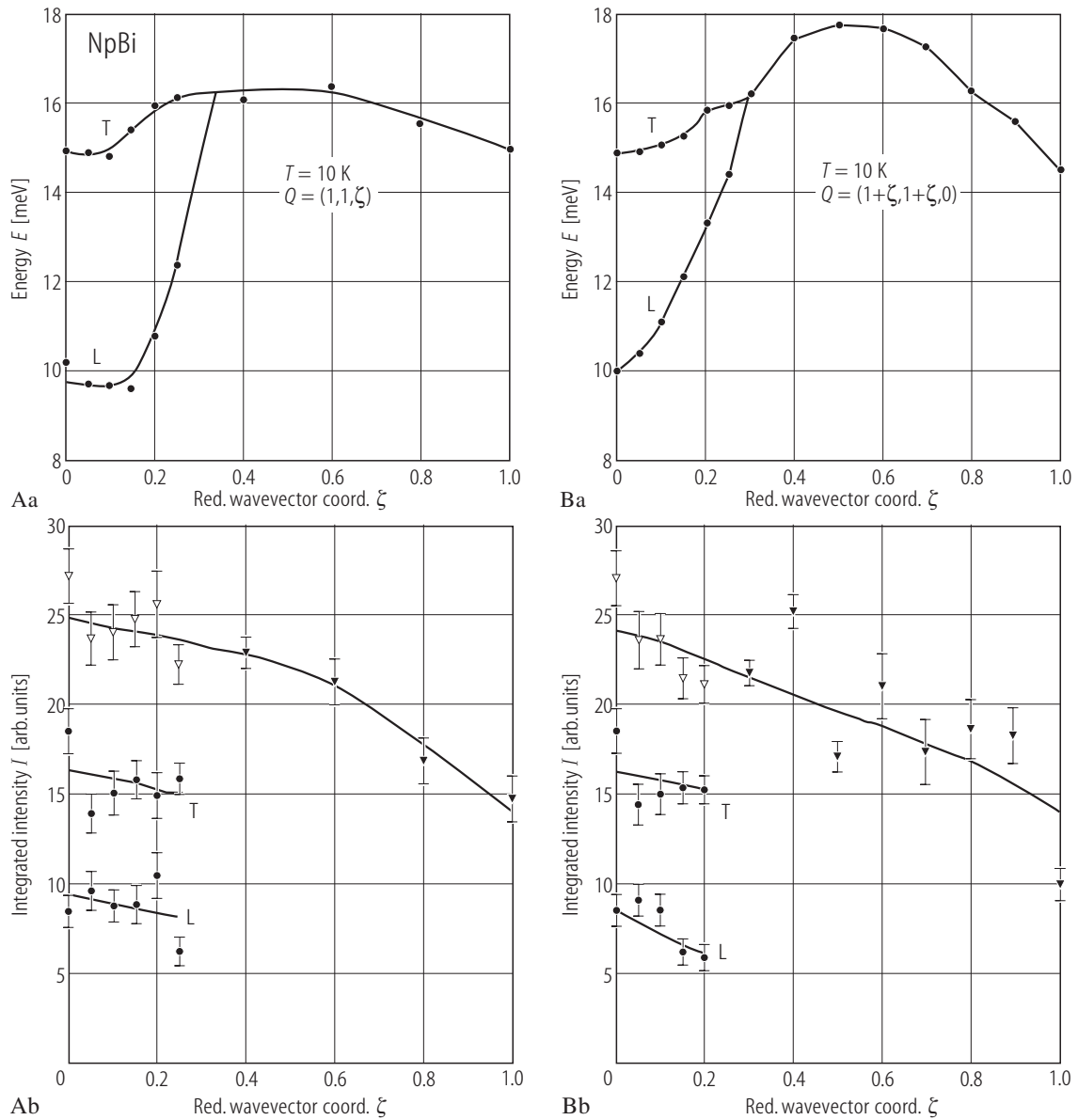


Fig. VI.8. NpBi s.c. Dispersion curves measured at 10 K along two directions: **(A)** $Q = (1, 1, \zeta)$ and **(B)** $Q = (1 + \zeta, 1 + \zeta, 0)$ (upper panels **(a)**) as well as integrated intensity (lower panels **(b)**) [97BBBF]. L and T denote longitudinal

and transverse modes. Open triangles correspond to the sum of the individual intensities of two peaks L and T. The filled symbols correspond to the observed peaks (see Fig.VI.6).

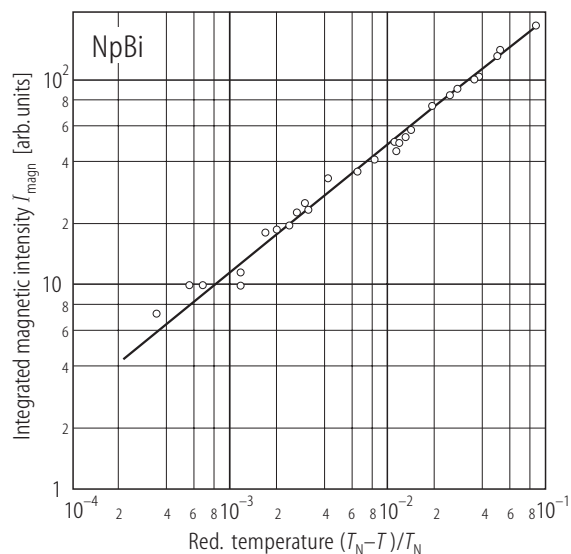


Fig. VI.10. NpBi s.c. Critical neutron scattering. The magnetic intensities, I_{magn} , vs. reduced temperature, $t = (T_N - T)/T_N$, as a log-log plot [92BBRS]. $T_N = 192.5(1)$ K, $\beta = 0.31(2)$.

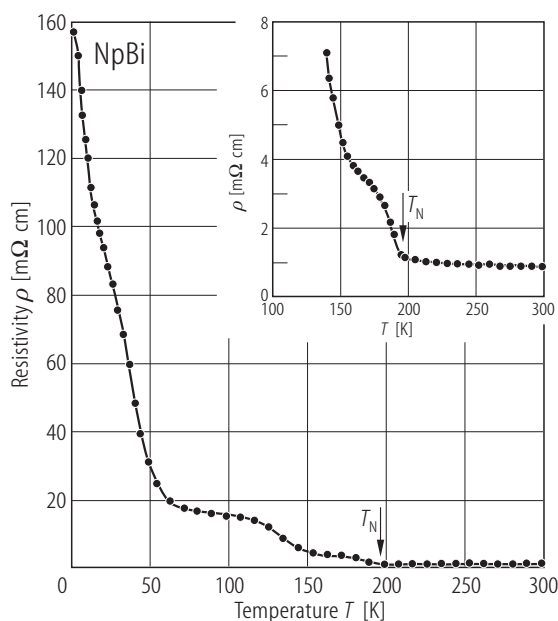


Fig. VI.11. NpBi. Electrical resistivity, ρ , vs. temperature, T [93FG]. Note that an increase in $\rho(T)$ occurs just below the temperature T_N ($= 193$ K), below which the triple- k , type I antiferromagnetic structure is formed. This is due to a strong reduction of charge carriers followed by the gap opening. In turn this causes an enormous increase of ρ up to 154 m Ω cm at 1.5 K, without sign of saturation. The inset shows the change in $\rho(T)$ in the region around T_N ($= 193$ K).

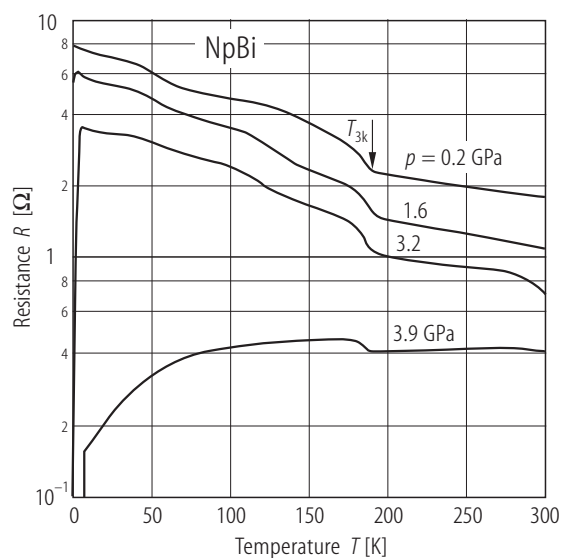


Fig. VI.12. NpBi s.c. Electrical resistance as $\log R$ vs. temperature, T , under pressures up to 3.9 GPa [97IZBS]. The sharp upturn in $\log R$ below T_{3k} ($= 88.5$ K) is associated with the onset of the $3k$ magnetic structure. T_{3k} decreases slightly under pressure.

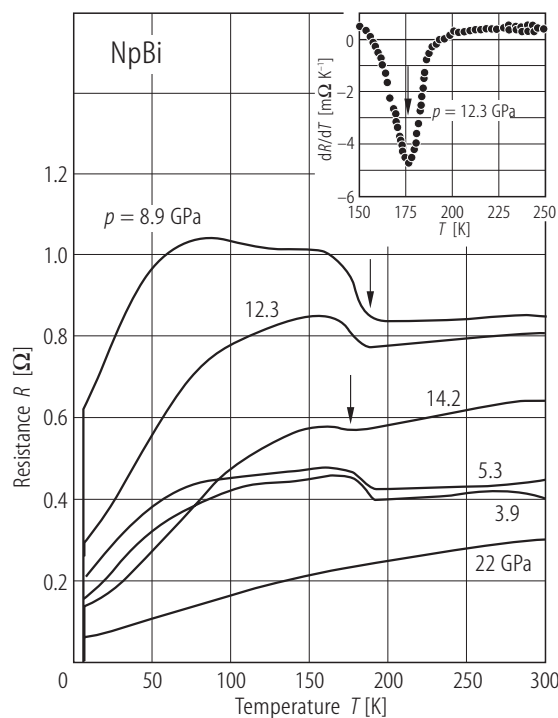


Fig. VI.13. NpBi s.c. Electrical resistance, R , vs. temperature, T , under pressures between 3.9 and 22 GPa [97IZBS]. The arrows point to the temperature of magnetic order at higher pressure. The rapid drop in the resistance above 3.9 GPa and below 10 K is due to traces of bismuth in the measured sample. The inset displays the temperature derivative of the resistance dR/dT vs. temperature, T , at 12.3 GPa.

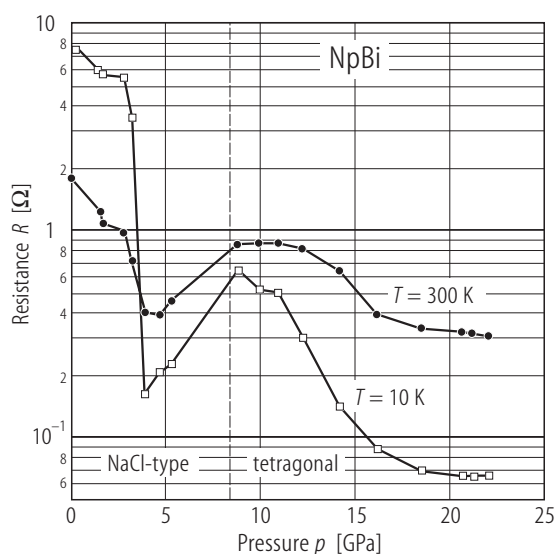


Fig. VI.14. NpBi s.c. Electrical resistance, R , measured at two temperatures: 10 K (open squares) and at 300 K (closed circles) [97IZBS]. The dashed line marks the structural transition reported in high-pressure X-ray measurements (see [93BH]).

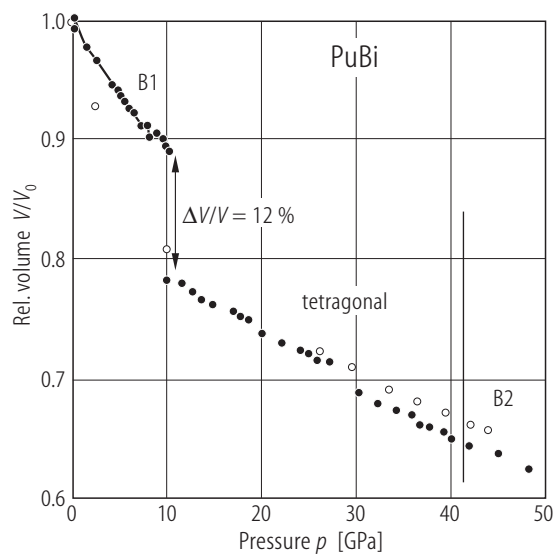


Fig. VI.15. PuBi. Relative volume, V/V_0 , vs. pressure, p , up to 50 GPa [99MHRR]. $a_0 = 0.63588(8)$ nm. Open circles increasing and closed circles decreasing pressures. The phase transitions from B1→tetragonal – (s.g. P4/mmm)→B2 appear at 10 and 42 GPa, respectively. If the first transition is accomplished by a 12% volume collapse, no change in volume is detected at the second transition. B_0 (= 61 GPa) and B'_0 (= 6.1) were calculated from the data below 10 GPa.

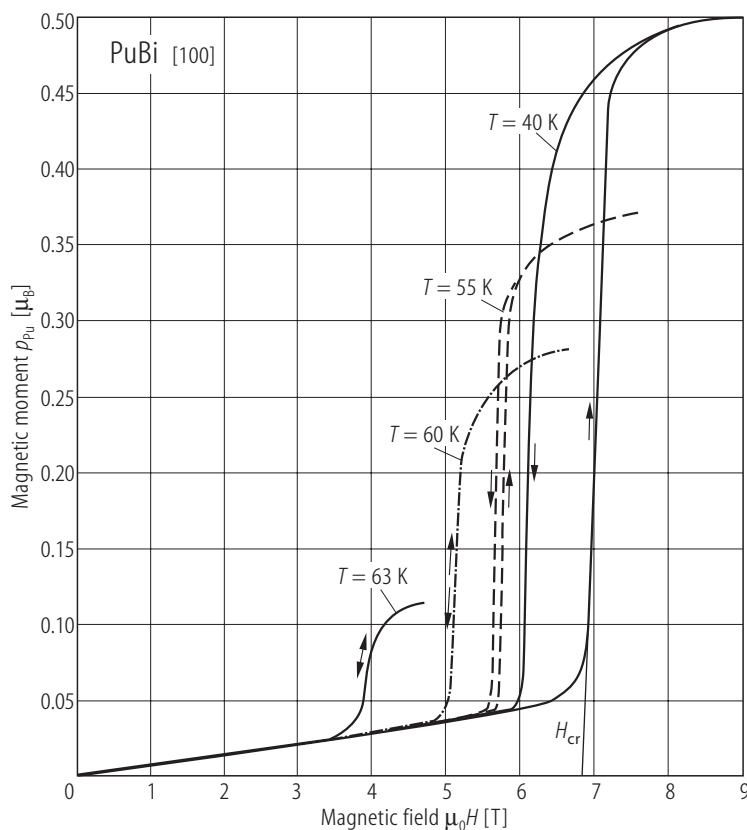
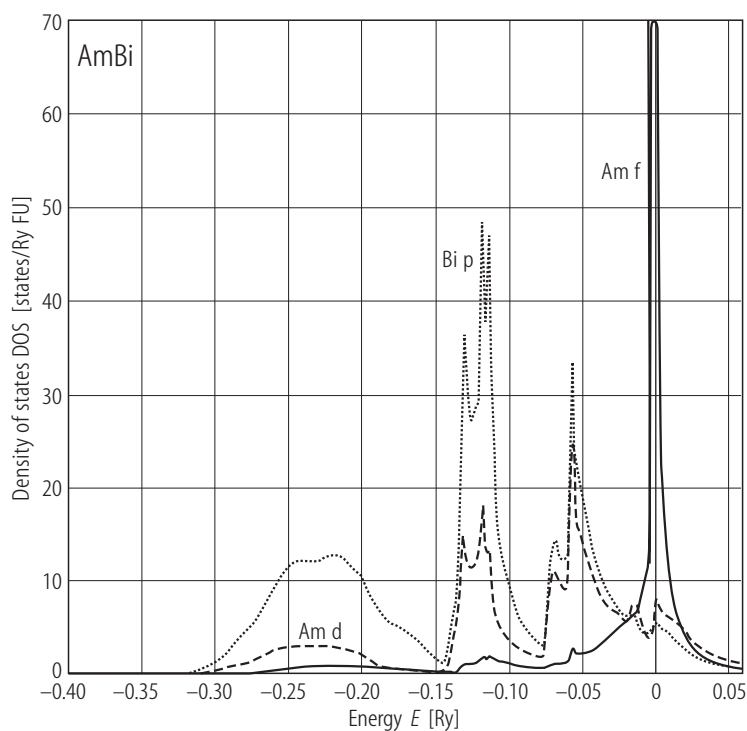


Fig. VI.16. PuBi. s.c. Magnetic moment p_{Pu} , vs. applied field, H , along the [100] axis for different temperatures [86MVSR2]. $T_N = 65$ K. Note meta-magnetic transitions with H_{cr} of 7 T at 40 K, which diminishes rapidly to 3.8 T at 63 K. This induced ferromagnetic phase aligns its moments ($p_s = 0.5(1) \mu_B$) along the [100] axis, which is an easy magnetization axis also for PuAs [86MVSR2] and for PuSb [83CTSM].



For Fig. VI.17 see next page

Fig. VI.18. AmBi. Partial DOS corresponding to the Bi p and Am d and f contributions obtained in the *ab initio* SIC-LSD approximation [01PSTS]. One observes that Am d states hybridize strongly with the p-band. In comparison with DOS of AmP, the difference exists in relation to DOS of AmBi. For the latter the p state moves up much more in energy and becomes less tightly bound to the nucleus. Also the f-peak is more narrowed due to larger Am-Am distance. In turn, the double f-peak structure originates from the p-f hybridization. For the energy band structure of AmBi calculated in LDA and LDA+ U approaches at the experimental lattice parameters see [05GDOB].

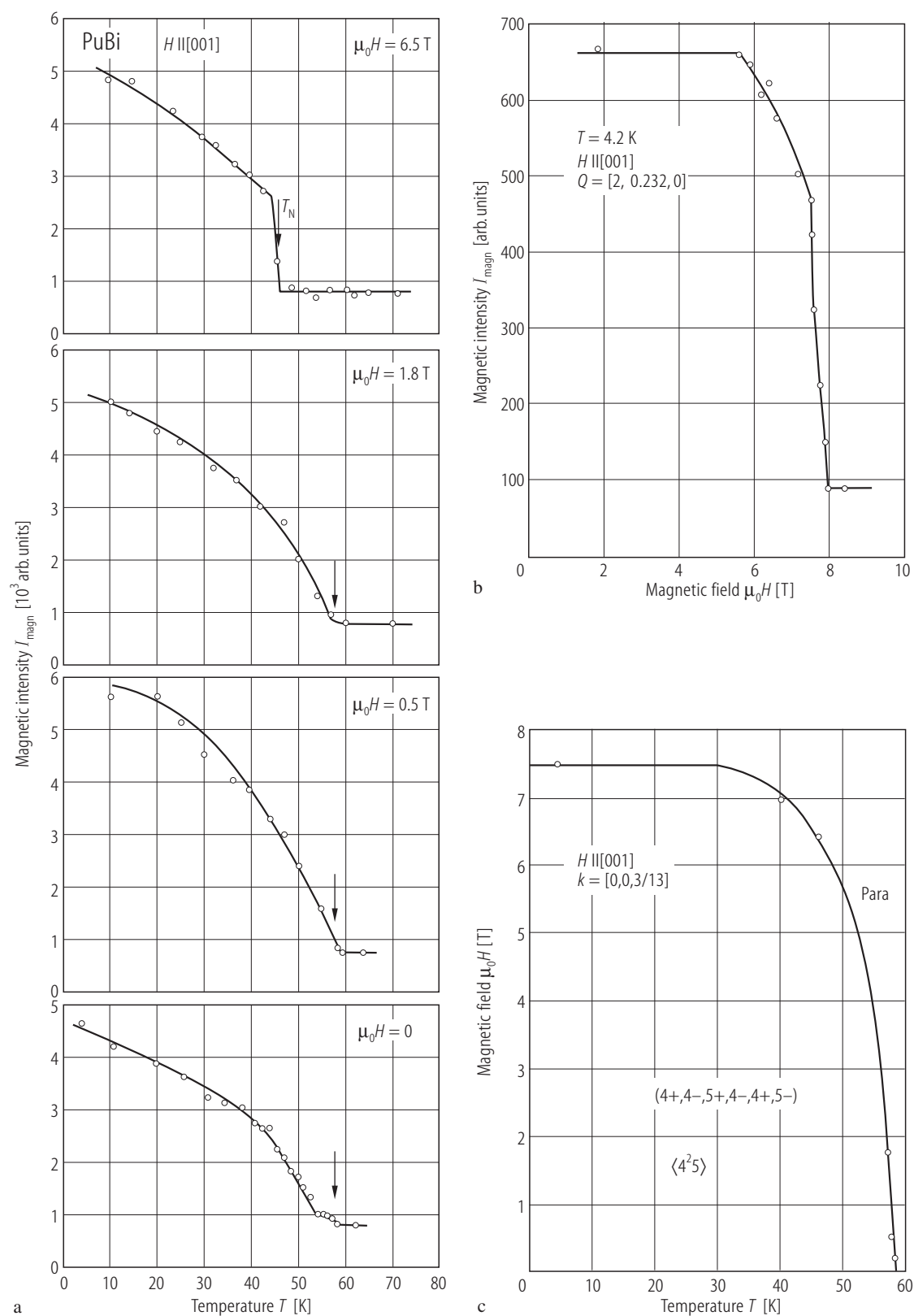
**Fig. VI.17.** For caption see next page.

Fig. VI.17. PuBi s.c. (a) Intensity of magnetic peak, $I_{\text{mag}}(2k0)$, vs. temperature, T , measured at different values of applied magnetic fields (as indicated) measured for the $H||[001]$ configuration [87BQRS]. At zero field $T_N = 58$ K and $k = [0,0,3/13]$. The wave vector k corresponds to the sequence of ferromagnetic (001) planes (4², 5), i.e. (4+, 4-, 5+, 4-, 4+, 5-), which yields a commensurate magnetic structure. At 4.2 K the magnetic structure is squaring up with $(m_k || k)$ and $m_k = 0.50 \mu_B$. The modulated phase is unaffected by the magnetic field. Note that the second-order transition at T_N becomes first order at fields as high as 6.5 T. Note also an accompanying decrease in T_N in this field. (b) Intensity of magnetic peak (2k0), at 4.2 K vs. magnetic field applied along [001] [87BQRS]. As seen, the antiferromagnetic magnetic structure is destroyed at 7.5 T and saturated paramagnetic state (induced ferromagnetism) is reached. (c) (H, T) MPD for $H||[001]$ [87BQRS]. Among the mononictides, PuBi is the only one which has the same magnetic structure over the whole temperature range up to T_N .

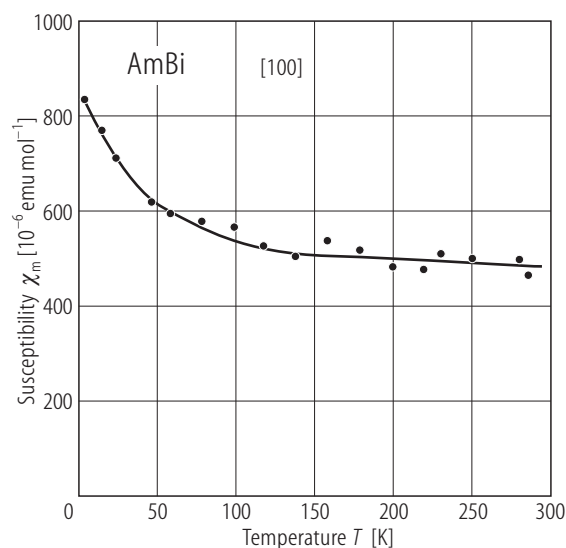
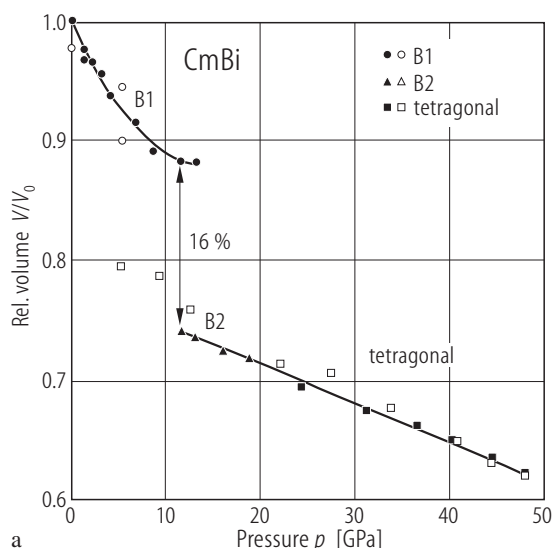


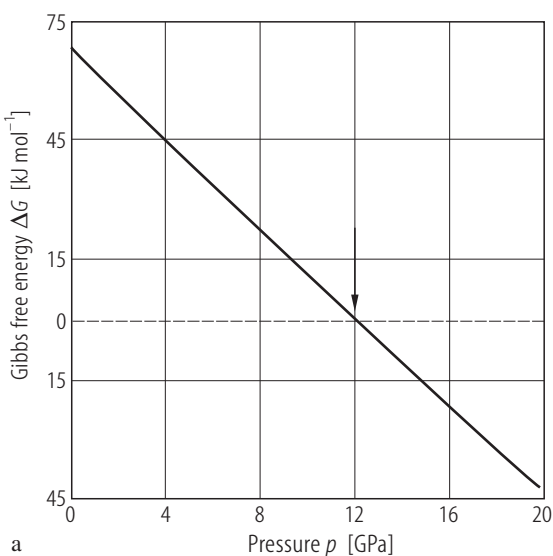
Fig. VI.20. CmBi. (a) Relative volume, V/V_0 , vs. pressure, p , up to 48 GPa [93GHBH]. $a_0 = 0.6328$ nm. Closed and open symbols indicate increasing and decreasing pressure, respectively. The phase transition from B1 to B2 takes place at 12 GPa. $B_0 = 53(3)$ GPa and $B'_0 = 8(2)$ (see also Table 7). Another transition to some tetragonal structure (s.g. P4/mmm) takes place at 19.6 GPa being a second-order transition to the distorted phase B2. Upon releasing pressure, the tetragonal lattice is retained down to 5 GPa and then below this pressure the structure is restoring directly to B1 omitting the B2-type. (b) Gibbs free energy, (ΔG), against pressure, p [03JS]. The high-pressure behaviour in CmBi is studied by a theoretical model based on an interatomic potential approach under the framework of charge transfer effects arising from three-body interaction. The calculated data for CmBi and those for UBi (see Fig. VI.4b) confirm the large volume change $\Delta V/V_0$ of 13.0 and 16.0% at the corresponding transition pressures, respectively, which is considered to be due to the delocalization of their 5f electrons. The theoretical results are in general in good agreement with the experimental data [93GHBH].

←

Fig. VI.19. AmBi s.c. Molar magnetic susceptibility, χ_m , vs. temperature, T , [92MV]. Note an almost temperature independent paramagnetism according to a $J = 0$ ground state of Am^{3+} .



a



a